Modeling and experimental study of an indirect evaporative cooler

Stefano De Antonellis [a,*], Cesare Maria Joppolo [a], Paolo Liberati [b], Samanta Milani [a], Francesco Romano [a]

[a] Dipartimento di Energia, Politecnico di Milano, Via Lambruschini, 4, 20156 Milan, Italy
[b] Recuperator S.p.A., Via Valfurva, 13, 20027 Rescaldina, MI, Italy

The use of indirect evaporative cooling technologies is an effective way to reach high energy efficiency systems and to reduce primary energy consumption. At present, interest in such systems is strongly increasing, with particular attention to data centers facilities. In fact, in these applications the indoor air temperature can be higher than the one of residential and commercial buildings, leading to a greater number of yearly operating hours of the system.

In this paper an indirect evaporative cooler, based on a cross flow heat exchanger, has been tested and modelled. Many experiments have been carried out in typical data centers operating conditions, varying both water flow rate and inlet air conditions. A phenomenological model of the indirect evaporative cooler has been developed: the model takes into account the effects of the adiabatic cooling of the secondary air stream in the inlet plenum and the actual wettability of the heat exchanger surface. The model has been extensively validated and it is shown that simulation results are in very good agreement with experimental data. Therefore, it can be a suitable tool to design and to predict performance of indirect evaporative cooling systems.

Keywords: Indirect evaporative, cooling Modeling, Experimental test, Wettability, Data center

1. Introduction

In recent years, demand of ICT services raised fast, leading to a significant increase in the number and size of data centers [1]. It has been estimated that in 2010 the worldwide electricity used by data centers was 1.3% of the total consumption [2] and that in 2012 it was around 270 TWh [3]. It is well known that in such facilities high heat fluxes should be dissipated: they can reach even 10 kW m^{-2}, leading to an electricity consumption for cooling up to 50% of the total consumption of the data center [1,2]. As a consequence, there is great interest from executive, technical and research personnel in improving both cooling system design and operation.

At present, buildings containing servers are mainly cooled through conventional vapour compression chillers. Recently, thermal ASHRAE guidelines for data centers [4], reporting appropriate temperature and humidity range for operation of ICT equipment, have been updated. The maximum allowable temperature, which should be properly selected in order to achieve energy savings and ICT equipment reliability, has been raised up even to 45 °C. Therefore, interest in application of free cooling technologies in data centers is rapidly increasing.

Article history:
Received 29 July 2016
Accepted 23 February 2017
Available online 1 March 2017

In the air to air indirect evaporative cooling systems, which are one of the most promising technologies, the primary air stream, which is supplied to the building, is cooled in a heat exchanger through a secondary air stream, which is humidified with liquid water. In case of data centers facilities, the system is generally arranged in recirculation mode: the primary air stream is extracted from the building while the secondary air stream is at outdoor conditions. An additional cooling system of the primary air stream is installed, in order to provide backup and peak load cooling capacity.

Currently, many research groups are working on indirect evaporative cooling systems [5], dealing with new thermodynamic cycles, heat exchanger materials and geometries, humidification systems and with the evaluation of energy savings compared to conventional devices. As summarized by Lin et al. [6], several models of indirect evaporate coolers based on cross-flow heat exchangers, which are widely used components, have been proposed in literature. Guo and Zhao [7] developed a one dimensional model, investigating the effects of many input parameters on system performance. Stoitchkov and Dimitrov [8] developed a short-cut method for calculating the effectiveness of a cross-flow IEC, introducing a correction to the Maclaine-cross and Banks' model [9]. Bolotin et al. [10] presented an ε-NTU analysis of two different

* Corresponding author.
E-mail address: stefano.deantonellis@polimi.it (S. De Antonellis).

Published Journal Article available at http://dx.doi.org/10.1016/j.enbuild.2017.02.057

Nomenclature

$A–C$	Experimental setup configuration
$A_{HE,net}$	Net heat exchanger cross area [m^2]
cp	Specific heat [J kg^{-1} K^{-1}]
$c_1–c_4$	Correlation parameters
Cw	Wettability coefficient
$D_1–D_3$	Setup geometric distances [m]
h	Net channel height [m]
H_{HE}	Heat exchanger height [m]
k	Thermal conductivity [W m^{-1} K^{-1}]
h_M	Convective mass transfer coefficient [kg s^{-1} m^{-2}]
h_T	Convective heat transfer coefficient [W m^{-2} K^{-1}]
$k_1–k_3$	Correlation parameters
$L_{HE}{}^*$	Net plates length and width [m]
$\dot{m}$	Specific flow rate [kg s^{-1} m^{-2}]
$\dot{M}$	Flow rate [kg s^{-1}]
N_{HE}	Number of heat exchanger plates [–]
pt	Plates pitch [m]
$\dot{Q}$	Volumetric flow rate [m^3 h^{-1}]
S1–S4	Numerical simulation conditions
T	Temperature [°C]
U_T	Overall heat transfer coefficient [W m^{-2} k^{-1}]
T0–T12	Experimental test conditions
v	Velocity [m s^{-1}]
x	Primary air flow direction [m]
x_i	Measured quantity [–]
X	Humidity ratio [kg kg^{-1}]
y	Secondary air flow direction [m]
y_i	Calculated quantity [–]

Greek letters

α, β	Correlation parameters
δ	Plates thickness [m]
δ_w	Water thickness [m]
ΔT	Temperature difference [°C]
ΔX	Humidity ratio difference [kg kg^{-1}]
ε_{db}	Dry bulb effectiveness [–]
ε_h	Saturation efficiency [–]
ρ	Density [kg m^{-3}]
σ	Wettability factor [–]
φ	Relative humidity [–]

Superscripts

N	Nominal condition ($\rho = 1.2$ kg m^{-3})

Subscripts

a	Air
HE	Heat exchanger
in	Inlet
out	Outlet
p	Primary air
s	Secondary air
sat	Saturation condition
v	Water vapour
w	Liquid water
W	Wall heat exchanger plates
wb	Wet bulb condition

Acronyms

EXP	Experimental
IEC	Indirect evaporative cooling
ICT	Information and communication technologies
NUM	Numerical

configurations of cross flow IEC, based on experimental tests provided by Martinez et al. [11]. Ren and Yang [12] discussed an analytical model of a parallel/counter-flow configuration of IEC, evaluating the effect of the wettability factor on performance. Heidarinejad and Moshari [13] developed the model proposed by Ren and Yang [12] to describe a sub-wet bulb indirect evaporative cooler. Hasan [14] presented a model for a sub-wet bulb IEC based on the ε-NTU method, using experimental data provided by Hsu et al. [15]. Finally, several works focus on the M-cycle or regenerative configurations: Anisimov et al. [16] evaluated performance of a system based on a cross flow heat exchanger, Pandelidis et al. [17] discussed the effect of different indirect evaporative coolers in desiccant cooling systems and Moshari et Heidarinejad [18] numerically studied a system for sub-wet bulb cooling. Anyway, these systems are not suitable for data centers: in fact, as previously described, in these applications the primary air flow of the IEC system is recirculated and it is completely separated from the secondary air stream.

It is well known that the variation of water flow rate has a significant effect on system performance [19]. In particular, the IEC system cooling capacity decreases significantly when the water flow rate cannot provide a satisfactory wettability of the heat exchanger surface. Furthermore, depending on the equipment setup, part of the supplied water can evaporate in the inlet plenum, leading to a pre-cooling and humidification of the secondary air stream which should be properly considered. Such effects have not been analyzed in detail in the existing literature. Therefore, the aim of this work is to develop an indirect evaporative cooling system model taking into account:

- The effect of adiabatic humidification of the secondary air stream in the inlet plenum.
- The wettability factor of the heat exchanger surface, as a function of the operating conditions of the system.

The research has been carried out through a detailed experimental analysis of the system. The model has been widely validated within and outside the calibration range and simulations have been performed to investigate primary air cooling in different working conditions of data centers.

2. Description of the investigated indirect evaporative cooling system

As shown in Fig. 1, the analyzed indirect evaporative cooling system consists of a commercial cross-flow plate heat exchanger, of n° 8 water spray nozzles installed in the upper part of the component and of an equipment to increase water pressure.

According to Fig. 1, the primary air stream is cooled in the heat exchanger at constant humidity ratio: it enters the system in condition *p,in* (indoor data center air condition) and it leaves the component in condition *p,out*. The secondary air stream, whose inlet condition is denoted as *s,in* (outside air condition), is supplied to the upper plenum where spray nozzles are installed. Due to the evaporation of water droplets, the secondary air stream is humidified almost at constant enthalpy and it reaches the heat exchanger face in condition *s,in,HE*, with higher humidity ratio and lower dry bulb temperature compared to the inlet condition *s,in*. Afterward, the secondary air stream passes through the heat exchanger and most water droplets impact on plate's surface. The further water evaporation leads to a reduction of the temperature of the secondary air stream, of the heat exchanger plates and of the primary air stream, which is the useful effect of the system. The secondary air stream leaves the system from the lower plenum in condition *s,out*.

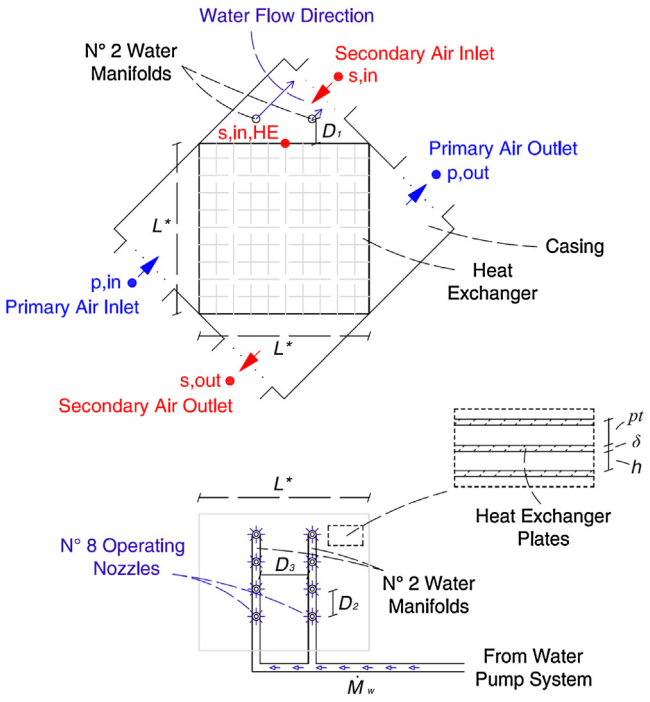

Fig. 1. Scheme of the investigated indirect evaporative cooling system.

Table 1
Main data of the investigated indirect evaporative cooling system.

Description	Parameter	Value
Number of plates	N_{HE}	119
Plate thickness	δ	0.14 mm
Plate pitch	pt	3.35 mm
Net channel height	$h = pt - \delta$	3.21 mm
Net plate length and width	L^*	470 mm
Plate conductivity	k_W	220 W m K^{-1}
Net face heat exchanger cross area	$A_{HE,net}$	0.089 m^2
Distance between manifolds and heat exchanger face	D_1	150 mm
Distance between nozzles	D_2	80 mm
Distance between manifolds	D_3	180 mm

Main characteristics of the cross flow heat exchanger are summarized in Fig. 1 and in Table 1.

The net face heat exchanger cross area $A_{HE,net}$, equal to 0.089 m^2, is evaluated as:

$$A_{HE,net} = \frac{\left(H_{HE} - N_{HE}\ \delta\right)\ L^*_{HE}}{2} \quad (1)$$

Where the heat exchanger height is $H_{HE} = (N_{HE}\text{-}1)\ pt + \delta$.

The plates (vertical installation) are made of aluminum alloy and their spacing is obtained through dimples with semispherical shape. The water is supplied to the secondary air stream through n° 8 nozzles, installed on two parallel manifolds (n° 4 nozzles on each manifold). The nominal water flow rate of each axial flow – full cone nozzle, provided by the manufacturer, is equal to 7.50 l h^{-1} at 9 bar.

Nozzles are installed in order to provide water in counter current arrangement respect to the secondary air stream, according to previous experimental results [19]. Finally, water is supplied to the nozzles through a commercial pumping unit, with maximum flow rate and pressure respectively equal to 110 l h^{-1} and 15 bar. In all tests the water is supplied directly from the municipal aqueduct without any recirculation, at an average temperature around 20 °C.

In this experimental and numerical work, the performance of the system is evaluated in terms of temperature difference (of both air streams) and of humidity ratio difference (of the secondary air stream) between the inlet and outlet of the heat exchanger. More precisely it is:

$$\Delta T_p = T_{p,in} - T_{p,out} \quad (2)$$

$$\Delta T_s = T_{s,in} - T_{s,out} \quad (3)$$

$$\Delta X_s = X_{s,out} - X_{s,in} \quad (4)$$

Finally, the specific water mass flow rate $\dot{m}_{w,in}$ is used as an indication of water supplied to the system, which is defined as:

$$\dot{m}_{w,in} = \frac{\dot{M}_{w,in}}{A_{HE,net}} \quad (5)$$

Where $\dot{M}_{w,in}$ is the total water mass flow rate.

Table 2
Sensors main data.

Abbreviation	Type of sensor	Accuracy[a]
T[b]	PT 100 Class A	±0.2 °C
RH[b]	Capacitive	±1% (between 0 and 90%)
p	Piezoresistive	±0.5% of reading ±1 Pa

[a] At T = 20 °C.
[b] Temperature and relative humidity probe.

3. Experimental set up, methodology and results

3.1. Experimental setup

3.1.1. General description of the test rig

Performance of the indirect evaporative cooling system has been evaluated through a specific experimental setup, which consists of the following parts:

- Two air handling units, which provide the primary and secondary air streams at the desired temperature, humidity ratio and flow rate.
- The indirect evaporative cooling system, as described in section 2, including ducts adopted for the connection with the air handling units and the necessary sensors to perform the performance measurement.

Main characteristics of temperature, relative humidity and pressure probes installed in the experimental setup are summarized in Table 2 and their position in the test rig is shown in Fig. 2.

3.1.2. Air handling units

The two air handling units are designed to control temperature, humidity and mass flow rate of primary and secondary air streams. Air conditions are controlled through heating coils, cooling coils, evaporative coolers and an electrical heater. Air flow rates are set by variable speed fans: the maximum primary air flow rate is 1400 m^3 h^{-1} and the maximum secondary air flow rate is 2000 m^3 h^{-1}. Each air flow rate is measured through two orifice plates, installed in two different parallel ducts, which are constructed according to technical standards [20]: air pressure drop across the orifices is measured by piezoresistive transmitters (Table 2). Depending on the desired supply air conditions, the system can work in outdoor air mode or in recirculation air mode. The water flow $\dot{M}_{w,in}$ supplied to the nozzles is measured through a turbine flow sensor, whose accuracy is ±3% of the reading.

It is highlighted that a detail description and a scheme of the test rig have been reported in previous works of the authors [21,22].

3.1.3. Indirect evaporative cooling equipment

Three different types of experimental tests have been performed in the present research work, in order to:

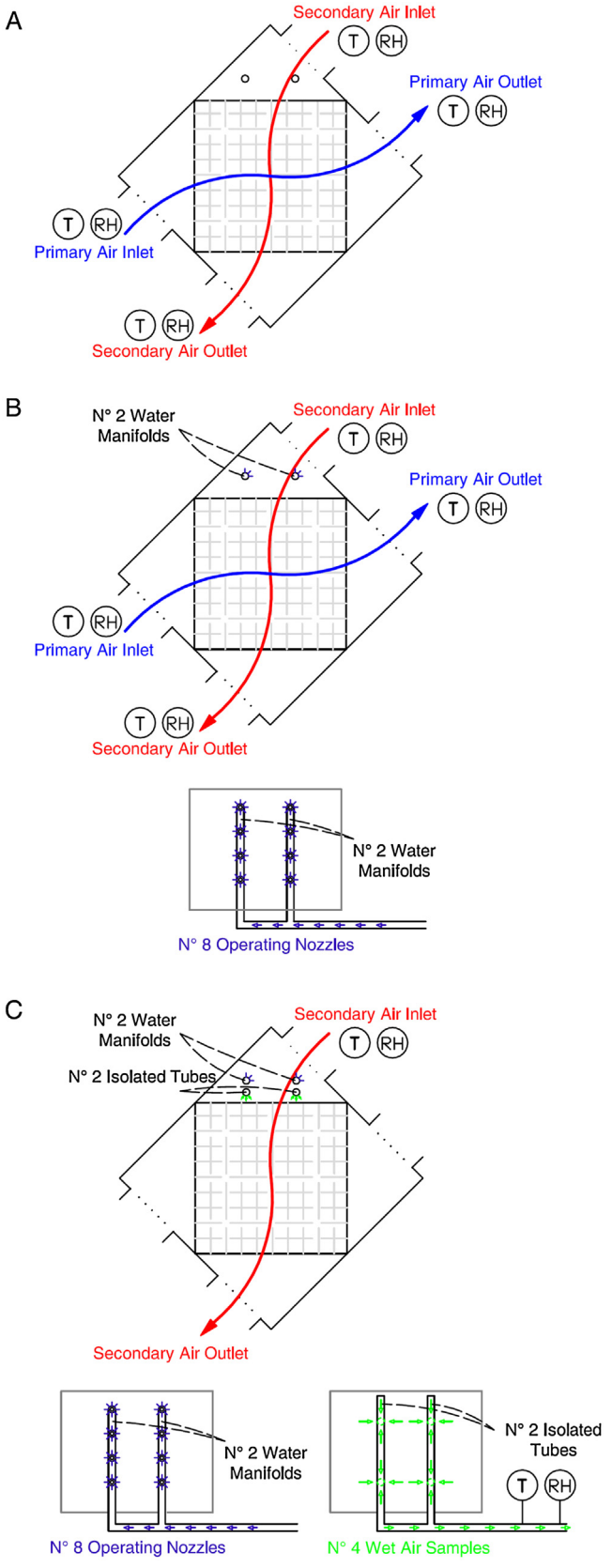

Fig. 2. Arrangement of the experimental setup of the indirect evaporative cooler adopted in tests.

- Evaluate outlet conditions and the performance of the heat exchanger in dry conditions, without secondary air humidification (Setup *A*).
- Evaluate outlet conditions and the performance of the complete indirect evaporative cooling system, with secondary air humidification (Setup *B*).
- Estimate the adiabatic humidification of the secondary air stream in the inlet plenum, before entering the heat exchanger (Setup *C*).

Therefore, the equipment has been connected to the two air handling units and arranged in three different configurations, as shown in Fig. 2. In the second case (Setup *B*), the arrangement was the same of the first one (Setup *A*), except for the water pumping system, which has been switched on in order to supply the water to the secondary air stream.

Temperature and humidity probes have been installed in the insulated ducts connecting the system with the air handling units: their position has been defined in order to reach a satisfactory air mixing. In addition, sensor measuring inlet conditions of the secondary air stream has been properly installed upstream the inlet plenum, in order to avoid influence of the humidification system.

In the last case (Setup *C*), the setup has been modified in order to evaluate the adiabatic humidification of the secondary air stream in the plenum. The apparatus consists of two insulated tubes, installed close to the heat exchanger face (at around 1 cm): n°2 holes have been created on the lowest part of each tube (n°4 holes in total) in order to sample a fraction of the secondary air stream. Average air condition is measured through a coupled temperature and relative humidity sensor. It is highlighted that such measurement is a very complex issue, in particular due to the following reasons: the limited available space in the casing, the not uniform air and water conditions, the presence of water droplets in the air and the field perturbation related to the introduction of sampling tubes in the plenum. In order to ascertain the absence of water droplet in the sampling tubes, a dry gauze has been inserted in the system (close to the holes), verifying no weight increase between the start and the end of each test.

In all cases, main data of the adopted sensors are summarized in Table 2.

3.2. Adopted experimental approach

In this work several tests have been carried out in order to evaluate performance of the indirect evaporative cooling system. A set of measured data has been used to calibrate the proposed model, while the remaining part has been used for its validation, as summarised in Table 3.

Air velocity v_a^N is referred to normal air condition ($\rho_a^N = 1.2\ \mathrm{kg\,m^{-3}}$) and calculated in this way:

$$v_a^N = \frac{\dot{Q}_a^N}{3600\ A_{HE,net}} \tag{6}$$

Where $\dot{Q}_a{}^N$ is the volumetric air flow rate in $\mathrm{m^3\,h^{-1}}$, referred to the aforementioned reference condition.

It is highlighted that tests *T0* deal with the characterization of the heat exchanger in dry conditions while tests *T1–T12* with the characterization of the indirect evaporative cooling system.

In each experimental session, data are collected in steady state conditions (300 samples of every physical quantity at a frequency of 1 Hz). Experimental uncertainty u_{xi} of each direct monitored variable x_i (T, φ and p) is:

$$u_{x_i} = \pm\sqrt{u_{x_{i,inst}}^2 + (t_{95}\ \ \sigma_{\overline{x_i}})^2} \tag{7}$$

Table 3
Summary of test conditions.

Test	IEC Setup[a]	Data usage[b]	$T_{s,in}$ [°C]	$X_{s,in}$ [g kg^{-1}]	v_s^N [m s^{-1}]	$T_{p,in}$ [°C]	$X_{p,in}$ [g kg^{-1}]	v_p^N [m s^{-1}]	$\dot{m}_{w,in}$ [kg s^{-1} m^{-2}]
T0	*A*	C	49.0–56.0	11.0	1.9–5.9	29.1–31.6	11.0	1.9–3.7	–
T1	*B, C*	C	30.0	10.6	3.7	35.0	10.0	3.7	0.09–0.19
T2	*B, C*	C	30.0	10.6	5.7	35.0	10.0	3.7	0.09–0.19
T3	*B, C*	C	30.0	13.4	3.7	35.0	10.0	3.7	0.09–0.19
T4	*B, C*	C	30.0	13.4	5.7	35.0	10.0	3.7	0.09–0.19
T5	*B, C*	C	36.8	10.6	3.7	35.0	10.0	3.7	0.09–0.19
T6	*B, C*	C	36.8	10.6	5.7	35.0	10.0	3.7	0.09–0.19
T7	*B*	V	30.0	10.6	4.7	35.0	10.0	3.7	0.09–0.19
T8	*B*	V	30.0	13.4	4.7	35.0	10.0	3.7	0.09–0.19
T9	*B*	V	36.8	10.6	4.7	35.0	10.0	3.7	0.09–0.19
T10	*B*	V	40.0	10.0	3.7	35.0	10.0	3.7	0.09–0.19
T11	*B*	V	30.0	10.0	3.7	30.0	10.0	3.7	0.09–0.19
T12	*B*	V	30.0	10.0	1.9	35.0	10.0	1.9	0.09–0.19

[a] According to Fig. 2.
[b] C: for model calibration; V: for model validation.

While generic combined uncertainty u_{yi} of calculated quantities y_i, such as ΔT_p, ΔT_s, and ΔX_s is calculated as:

$$u_{y_i} = \sqrt{\sum_i \left(\frac{\partial y_i}{\partial x_i} u_{x_i,inst}\right)^2 + t_{95}^2 \sum_i \left(\frac{\partial y_i}{\partial x_i} \sigma_{\overline{x_i}}\right)^2} \quad (8)$$

Where $u_{xi,inst}$ is the instrument uncertainty of the measured quantity, t_{95} is the student test multiplier at 95% confidence and $\sigma_{\overline{x_i}}$ is the standard deviation of the mean. The methodology and the assumptions are estimated in accordance with the reference international standard [23].

4. Experimental analysis

Results of tests *T0* and *T1–T6*, which have been used to calibrate the model as reported in Section 6, are preliminarily discussed. In particular, effectiveness of the heat exchanger in dry conditions, performance of the indirect evaporative cooling system and humidification effect in the secondary air inlet plenum are evaluated.

4.1. Heat exchanger in dry conditions

Preliminary tests in dry conditions (test *T0*, Table 3) have been performed with the aim of evaluating the reference effectiveness of the heat exchanger. The dry bulb effectiveness ε_{db} is defined as:

$$\varepsilon_{db} = \frac{\dot{M}_p cp_p \left(T_{p,in} - T_{p,out}\right)}{\left(\dot{M}cp\right)_{min} \left(T_{p,in} - T_{s,in}\right)} \quad (9)$$

Where, according to the conditions of the tests, the thermal capacity of the secondary air stream is equal or higher than the one of the primary air flow ($\dot{M}_s cp_s \geq \dot{M}_p cp_p$).

The measured dry bulb effectiveness ε_{db} varies between 62.9% (at $v_s^N = v_p^N = 1.9$ m s^{-1}) and 62.1 % (at $v_s^N = v_p^N = 3.7$ m s^{-1}), when $T_{p,in}$ and $T_{s,in}$ are respectively around 31 °C and 50 °C. Finally, it is highlighted that the nominal pressure drop across the heat exchanger is 100 Pa when $v_a = 3.2$ m s^{-1} and $T_a = 35$ °C.

4.2. Indirect evaporative cooling system

In the present analysis, it is assumed that the primary and secondary air flows entering the system are respectively at data center indoor air conditions ($T_{p,in}$) and at outside air conditions ($T_{s,in}$). The experimental tests *T1–T6* have been operated through the setup arrangement *B*, described in Fig. 2, in representative conditions of data center applications. More precisely, the air from the data center is kept at constant temperature, humidity and flow rate, namely $T_{p,in} = 35$ °C, $X_{p,in} = 10$ g kg^{-1} and $v_p^N = 3.7$ m s^{-1}. Instead, secondary air conditions have been properly controlled in order to compare directly different experimental results: in each set of test, the inlet air dry bulb temperature, the wet bulb temperature, the humidity ratio, the air velocity and the water flow rate have been varied independently.

Experimental results of tests *T1–T6* have already been discussed in detail in a previous work of the authors [19]. Therefore, in this section performance are briefly resumed in terms of temperature difference of both air streams and of humidity ratio difference of the secondary air one. In Fig. 3, the effect of the variation of one inlet condition at a time is put in evidence. In the analyzed working conditions it is:

- The higher the water flow rate, the higher the humidification of the secondary air stream and, therefore, the higher the primary air temperature reduction ΔT_p.
- An increase in the humidity ratio of the secondary air stream $X_{s,in}$ at constant dry bulb temperature $T_{s,in}$ (*T3* and *T4* compared to *T1* and *T2*) leads to a reduction of ΔX_s and, as a consequence, of ΔT_p.
- An increase in the dry bulb temperature $T_{s,in}$ at constant humidity ratio $X_{s,in}$ (*T5* and *T6* compared to *T1* and *T2*) or at constant wet bulb temperature $T_{wb,s,in}$ (*T5* and *T6* compared to *T3* and *T4*) leads to a significant increase in ΔX_s (due to the lower inlet relative humidity) and, as a consequence, of ΔT_s. Anyway, due to the higher secondary air average temperature in the heat exchanger, the reduction of the process air temperature is lower.
- Finally, an increase in the secondary air flow rate (*T2* compared to *T1*, *T4* compared to *T3* and *T6* compared to *T5*) leads to an increase in ΔT_p in case of low secondary air inlet temperature and high water mass flow rate.

4.3. Direct saturation efficiency of secondary air stream

Tests about the secondary air humidification at the inlet plenum of the IEC systems have been performed through the configuration *C* of the experimental setup described in Fig. 3. The experiments have been performed in conditions *T1–T6*, as reported in Table 3, and humidification is evaluated in term of direct saturation efficiency ε_h, defined as:

$$\varepsilon_h = \frac{T_{s,in} - T_{s,in,HE}}{T_{s,in} - T_{wb,s,in}} \cong \frac{X_{s,in} - X_{s,in,HE}}{X_{s,in} - X_{wb,s,in}} \quad (10)$$

Thus the saturation efficiency is most frequently defined on temperature [24], in this work it has been calculated from air humidity ratio in order to exclude the effect related to air cooling or heating in the sampling system, which could lead to incorrect results.

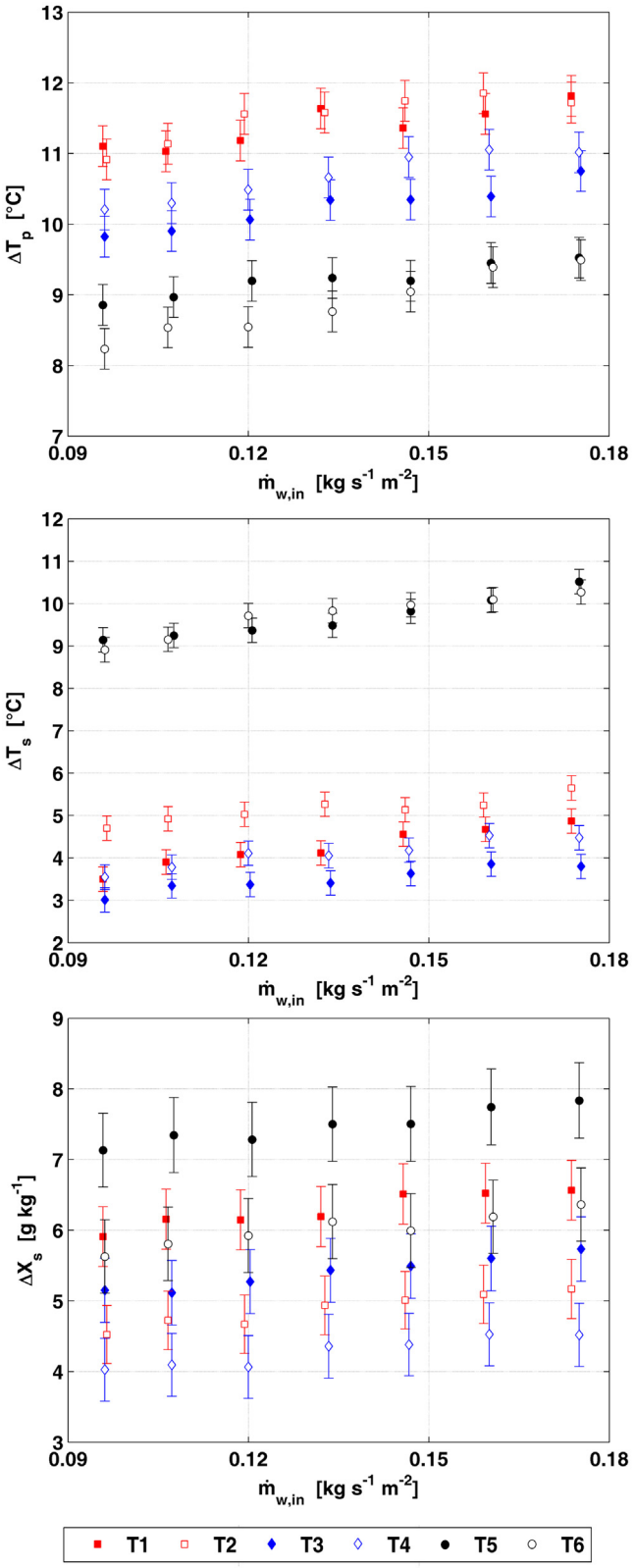

Fig. 3. Experimental results of the indirect evaporative cooling system in tests *T1–T6* (Table 3).

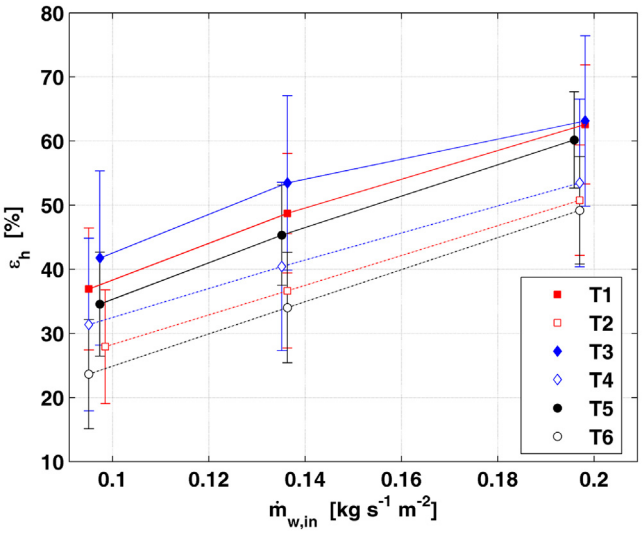

Fig. 4. Experimental saturation efficiency in the secondary air plenum in tests *T1–T6* (Table 3).

Referring to the experimental results reported in Fig. 4, it is possible to state that:

- The higher the water flow rate, the higher the heat and mass exchange area and, therefore, the saturation efficiency.
- The higher the air flow rate, the lower the air residence time and, as a consequence, the saturation efficiency.
- The saturation efficiency is slightly dependent on inlet air condition. The higher the difference between dry and wet bulb temperature, the higher the amount of water that should evaporate to reach saturation condition. In this case, due to the small water to air mass flow ratio ($1.3\% < \dot{M}_w/\dot{M}_a < 4.2\%$), the heat and mass transfer interface area decreases more significantly during the evaporation process, leading to a lower saturation efficiency.

5. Model description

The model of the indirect evaporative cooler discussed in this work is based on the one proposed by Ren and Yang [12]. The following assumptions have been adopted in this study:

1. Steady-state conditions.
2. No heat losses to the surroundings.
3. Negligible axial heat conduction and water diffusion in the air streams.
4. Negligible heat conduction in the heat exchanger plates.
5. Uniform air inlet conditions.
6. Interface plate temperature is equal to bulk water temperature.
7. Constant Lewis number.

According to Fig. 5, energy and water mass balances have been applied to an infinitesimal element of the heat exchanger. Governing equations are hereinafter reported:

Energy balance in the primary air stream:

$$\frac{dT_p}{dx} = \frac{U_{T,p}\left(T_W - T_p\right)}{v_p cp_p \rho_p \frac{h}{2}} \tag{11}$$

Energy balance in the secondary air stream:

$$\frac{dT_s}{dy} = \frac{h_{T,s}\left(T_W - T_s\right)}{v_s cp_s \rho_s \frac{h}{2}} + \frac{h_{M,s}\left(\lambda + cp_s T_s\right)\left(X_W - X_s\right)\quad \sigma}{v_s cp_s \rho_s \frac{h}{2}} \tag{12}$$

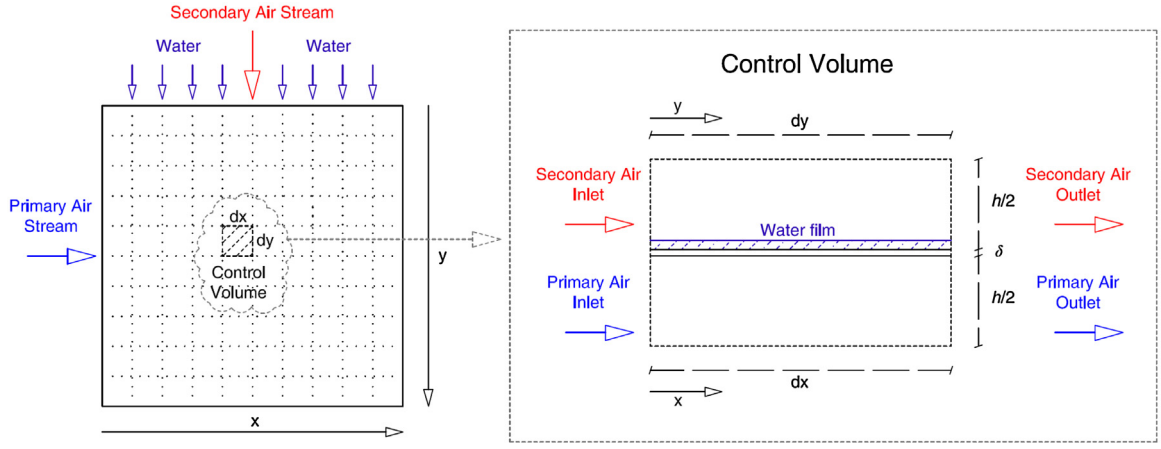

Fig. 5. Scheme of the heat exchanger and of the control volume.

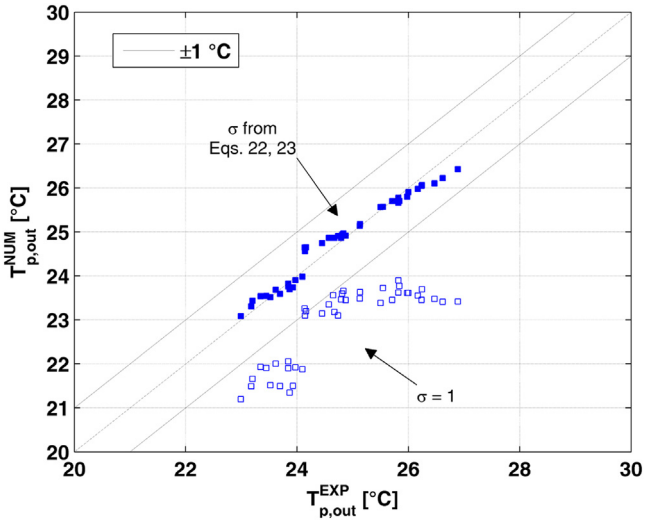

Fig. 6. Parity plot between experimental and numerical $T_{p,out}$. Results with $\sigma = 1$ and with σ determined through the proposed correlations. Tests *T1–T6* (Table 3).

Water mass balance in the secondary air stream:

$$\frac{dX_s}{dy} = \frac{h_{M,s}\,(X_W - X_s)\quad \sigma}{v_s \rho_s \frac{h}{2}} \tag{13}$$

Energy balance in the interface and water layer:

$$h_{M,s}\,(\lambda + cp_s T_s)(X_s - X_W)\quad \sigma + h_{T,s}\,(T_s - T_W) + U_{T,p}\left(T_p - T_W\right) = 0 \tag{14}$$

Water mass balance in the water film:

$$\frac{d\dot{m}_w}{dy} = \frac{h_{M,s}\,(X_s - X_W)\quad \sigma}{h/2} \tag{15}$$

Where σ is the ratio between the actual wet surface area of the control volume and its total area and $U_{T,p} = 1/(1/h_{T,p} + \delta/k_W)$. Instead, the mass transfer coefficient is calculated in the following way, assuming $Le = 1$:

$$h_M = \frac{h_T}{cp_a} \tag{16}$$

It is highlighted that v_p and v_s are assumed constant and calculated respectively as $v_p = v_p{}^N\ \rho_a{}^N/\rho_{p,in}$ and as $v_s = v_s{}^N\ \rho_a{}^N/\rho_{s,in}$. The humidity ratio at wall is calculated as:

$$X_W = 0.622\,\frac{1}{\frac{p_{tot}}{p_{v,sat}} - 1} \tag{17}$$

Where the total atmospheric pressure p_{tot} has been assumed constant and equal to 101325 Pa and the water vapour saturation pressure $p_{v,sat}$ is calculated with Eq. (18):

$$p_{v,sat} = e^{23.196 - \frac{3816}{T_W + 273.15 - 46.13}} \tag{18}$$

Finally, according to Fig. 1, boundary conditions are $T_p\ (x=0) = T_{p,in}$, $T_s\ (y=0) = T_{s,in,HE}$, $X_s\ (y=0) = X_{s,in,HE}$ and $\dot{m}_w\ (y=0) = \dot{m}_{w,in,HE}$ (where $\dot{m}_{w,in,HE} = \dot{m}_{w,in} - (X_{s,in,HE} - X_{s,in})\ v_s{}^N\ \rho^N$ is the water specific mass flow rate net of the water evaporation in the secondary air inlet plenum). Finally, $T_{p,out}$, $T_{s,out}$ and $X_{s,out}$ are calculated as average values at the heat exchanger outlet section.

6. Model calibration

6.1. Convective heat transfer coefficient

As described in Section 2, the heat exchanger is made of aluminium alloy plates with surface dimples. It is well known that such protrusions lead to a higher heat transfer coefficient compared to a smooth surface, both in laminar [25] and turbulent [26] flow conditions. Heat transfer strongly depends on surface geometry (such as dimples depth, pitch, diameter and location) and channel height. For this reason a specific correlation to estimate heat transfer coefficient of the analyzed heat exchanger has been developed. The form of the equation to calculate h_T is:

$$h_T = \frac{k_a}{2\ h}\,\alpha\, Re^{\beta}\, Pr^{1/3} \tag{19}$$

Where k_a is the thermal conductivity of air, $2\,h$ is the hydraulic diameter of the channel, *Re* and *Pr* are respectively the Reynolds and Prandlt number. The two parameters α and β have been calculated by minimizing the error between the dry bulb effectiveness measured in test *T0* and the corresponding one calculated through the numerical model. Resulting values are $\alpha = 0.0185$ and $\beta = 0.928$. In the investigated working conditions, with Reynolds number between 700 ($v_s{}^N \approx 1.8\,\mathrm{m\,s^{-1}}$) and 2300 ($v_s{}^N \approx 5.9\,\mathrm{m\,s^{-1}}$), differences between measured and calculated dry bulb effectiveness are always within 0.6 %.

6.2. Secondary air saturation efficiency

Secondary air inlet conditions $T_{s,in,HE}$ and $X_{s,in,HE}$ are calculated from the saturation efficiency defined in Eq. (10). As shown in detail in Section 4.3, values of ε_h of the investigated indirect evaporative cooling system strongly depend on the secondary air inlet conditions and on the water flow rate. According to the considerations

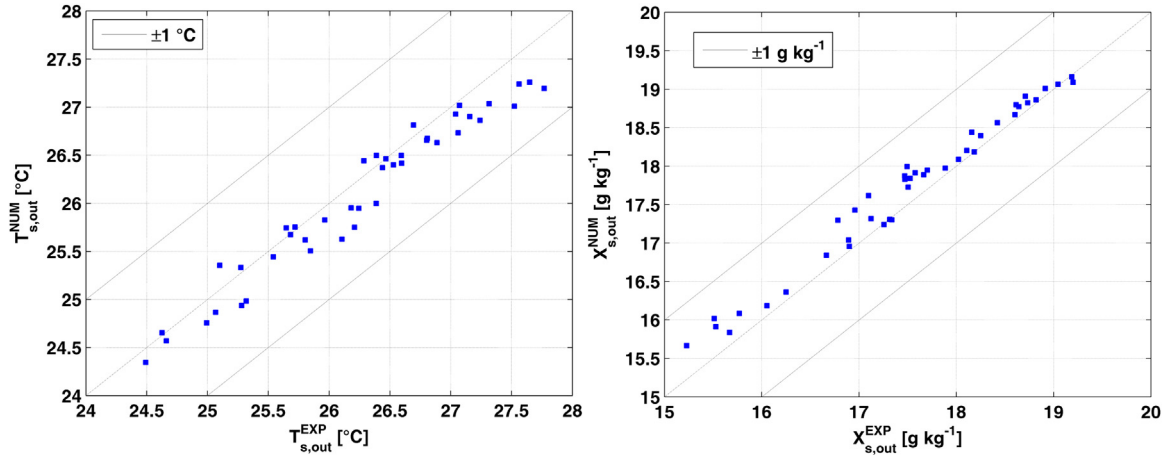

Fig. 7. Parity plot of numerical and experimental Ts,out and Xs,out in tests *T1–T6* (Table 3).

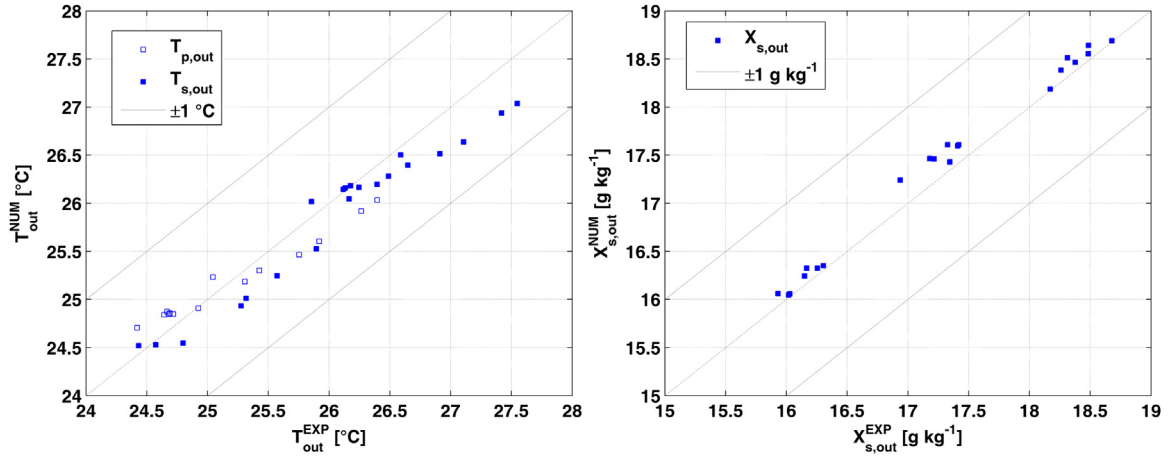

Fig. 8. Parity plot of numerical and experimental $T_{p,out}$, $T_{s,out}$ and $X_{s,out}$ in tests *T7–T9* (Table 3).

reported in Section 4.3, in this work the following correlation to predict the saturation efficiency is proposed:

$$\varepsilon_h = \frac{c_1 \ln\left(T_{s,in} - T_{s,wb,in}\right) + c_2}{\dot{M}_s^{c_3}} \dot{M}_{w,in}^{c_4} \tag{20}$$

Where the terms c_1–c_4 have been calculated by minimizing the error between the calculated and the measured saturation efficiency in conditions of tests *T1–T6*. The adopted coefficients are $c_1 = -1.2606$, $c_2 = 8.9481$, $c_3 = 0.6717$ and $c_4 = 0.7396$. The average difference between the calculated and measured efficiency $|\varepsilon_h{}^{NUM} - \varepsilon_h{}^{EXP}|$ in tests *T1–T6* is 11.8%. In addition, the calculated values of ε_h are always within the experimental uncertainty of the measured ones.

6.3. Surface wettability factor

Surface wettability factor σ is a crucial issue that should be properly taken into account in indirect evaporative cooling systems modeling. Thus in several models available in literature the effect of the wettability factor on performance is discussed, no information is provided to correlate σ to actual system operating conditions and, in particular, to the secondary air and water flow rate. In Fig. 6, it is shown that the outlet primary air temperature calculated with the model with $\sigma = 1$ is systematically underestimated compared to the experimental results (from 0.9 °C to 3.5 °C). Therefore, a correlation to satisfactorily predict the wettability factor is necessary.

In the inlet section of the heat exchanger, assuming that there are not water droplets in the air stream, the wettability factor in each plate can be calculated as:

$$\sigma = \frac{\dot{m}_w \quad L^* h}{2 \quad L^* \delta_w \nu_w \rho_w} \tag{21}$$

The estimation of the average water thickness and velocity is very difficult and depends strongly on operating conditions. Therefore, Eq. (21) can be rearranged in this form:

$$\sigma = \dot{m}_w \frac{h}{2 \quad \delta_w \nu_w \rho_w} = \dot{m}_w \quad C_w \tag{22}$$

The term C_w is a coefficient which is a function of the specific inlet water flow rate and of the secondary air velocity. The correlation adopted to calculate C_w is:

$$C_w = \frac{k_1}{\nu_S^N k_2 e^{k_3 \quad \dot{m}_{w,in,HE}}} \tag{23}$$

Where $k_1 = 8.0250$, $k_2 = 0.305$ and $k_3 = 7.2$ and $\dot{m}_{w,in,HE} = \dot{m}_{w,in} - (X_{s,in,HE} - X_{s,in})\, v_s{}^N\, \rho^N$ is the water specific mass flow rate net of the water evaporation in the secondary air inlet plenum. The value of $X_{s,in,HE}$ is calculated with Eq. (10). It is highlighted that an increase in $v_s{}^N$ leads to a higher dragging of water droplets and, as a consequence, to a reduction in C_w and σ. Instead, the higher $\dot{m}_{w,in,HE}$, the higher the impact of water droplets on secondary air inlet plenum walls and, therefore, the lower the coefficient C_w. Anyway, accord-

ing to Eq. (22), it is worth specifying that an increase in $\dot{m}_{w,in,HE}$ generally leads to an increase in σ.

The term C_w is calculated one time at inlet heat exchanger conditions (Eq. (23)) while σ is calculated in each control volume as a function of C_w and the actual water flow rate $\dot{m}_w$ (Eq. (22)). The form of Eq. (23) and coefficients k_1-k_3 have been determined in order to minimize the squared mean root difference between the calculated and measured outlet process temperature in tests *T1 – T6* (Table 3).

As shown in Fig. 6, the maximum difference between the outlet primary air temperature calculated with the proposed correlation and experimental values is 0.51 °C, being significantly lower than the one obtained with $\sigma = 1$.

It is worth to specify that the proposed model is accurate in the prediction of the secondary air outlet conditions too. In Fig. 7, measured and calculated outlet temperature and humidity ratio are reported: the maximum values of $|{T_{s,out}}^{NUM} - {T_{s,out}}^{EXP}|$ and $|{X_{s,out}}^{NUM} - {X_{s,out}}^{EXP}|$ are respectively equal to 0.6 °C and 0.5 g kg^{-1}.

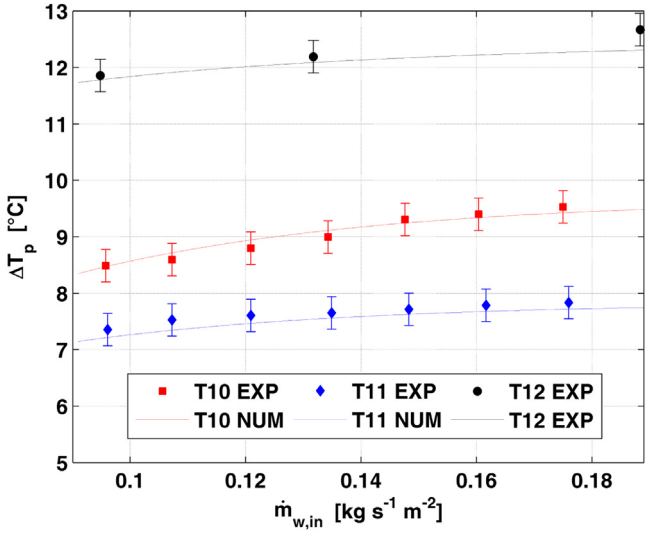

Fig. 9. Primary air temperature reduction: comparison between numerical and experimental results in tests *T10–T12* (Table 3).

7. Model validation

The indirect evaporative cooler model described in Sections 5 and 6 has been widely validated in different operating conditions. Simulation results are compared with experimental data in conditions of tests *T7–T9*, which have not been used in the model calibration process. In these tests, operating conditions are the same of tests *T1–T6*, except for the secondary air velocity ${v_s}^N$, which is equal to 4.7 m s^{-1} instead of 3.7 or 5.7 m s^{-1}. Therefore, it is possible to state that conditions of tests *T7–T9* are within the adopted calibration range.

In Fig. 8, it is highlighted that the maximum differences between numerical and experimental results of $T_{p,out}$, $T_{s,out}$ and $X_{s,out}$ are respectively 0.36 °C, 0.51 °C and 0.3 g kg^{-1}.

Finally, simulation results are compared with a further set of experimental data collected in operating conditions outside tha calibration range. In particular, $T_{s,in}$ in test *T10* has been increased up to 40 °C, $T_{p,in}$ in test *T11* has been reduced to 30 °C and air velocity of both air streams is reduced in test *T12* (${v_p}^N = {v_s}^N = 1.9$ m s^{-1}). In all cases $X_{s,in}$ is around 10 g kg^{-1}.

As shown in Fig. 9, numerical results are in very good agreement with experimental data, even in test *T12*, whose operating conditions are far from the model calibration range.

8. Parametric analysis

In this section simulations have been carried out to evaluate indirect evaporative cooling performance in different operating conditions, as summarized in Table 4. Results are shown in terms of ΔT_p for different secondary air stream conditions.

In Fig. 10 it is shown that when $T_{p,in}$ is equal to 35 °C, the primary air temperature reduction can reach 17 °C at low secondary air temperature and humidity ratio. In case of hot and humid climate (such as $T_{s,in} = 40$ °C and $X_{s,in} = 14$ g kg^{-1}) ΔT_p is still higher than 7 °C. Finally, with the adopted water flow rate ($\dot{m}_{w,in} = 0.14$ kg s^{-1} m^{-2}), an increase in ${v_s}^N$ (simulation *S2* compared to *S1*) is useful only in case of low temperature and humidity ratio of the secondary air stream, as discussed in detail in a previous work [19].

In Fig. 11 simulations with $T_{p,in}$ equal to 25 °C are reported. In this case, results show that ΔT_p of the primary air is significantly lower compared to the previous case, due to the lower average temperature difference between the primary and secondary air stream. In the analyzed conditions, the maximum ΔT_p is slightly higher than 9 °C: it is highlighted that in hot and humid climate conditions, the primary air stream is even heated.

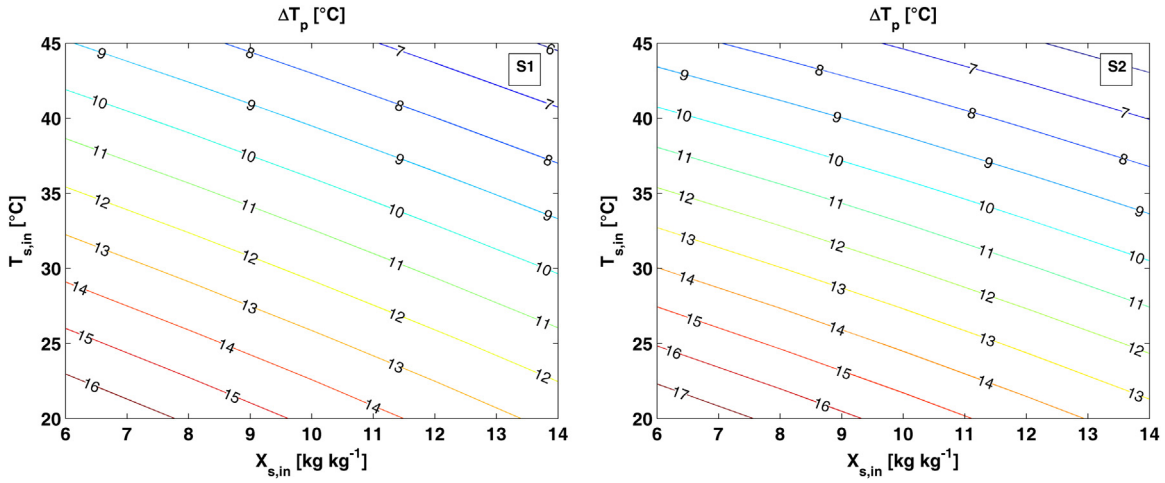

Fig. 10. Numerical results in conditions S1 and S2 (Table 4).

Table 4
Summary of simulations.

Simulation	$T_{s,in}$ [°C]	$X_{s,in}$ [g kg^{-1}]	v_s^N [m s^{-1}]	$T_{p,in}$ [°C]	$X_{p,in}$ [g kg^{-1}]	v_p^N [m s^{-1}]	$\dot{m}_{w,in}$ [kg s^{-1} m^{-2}]
S1	20.0–45.0	6.0–14.0	3.7	35	10.0	3.7	0.14
S2	20.0–45.0	6.0–14.0	5.7	35	10.0	3.7	0.14
S3	20.0–45.0	6.0–14.0	3.7	25	10.0	3.7	0.14
S4	20.0–45.0	6.0–14.0	5.7	25	10.0	3.7	0.14

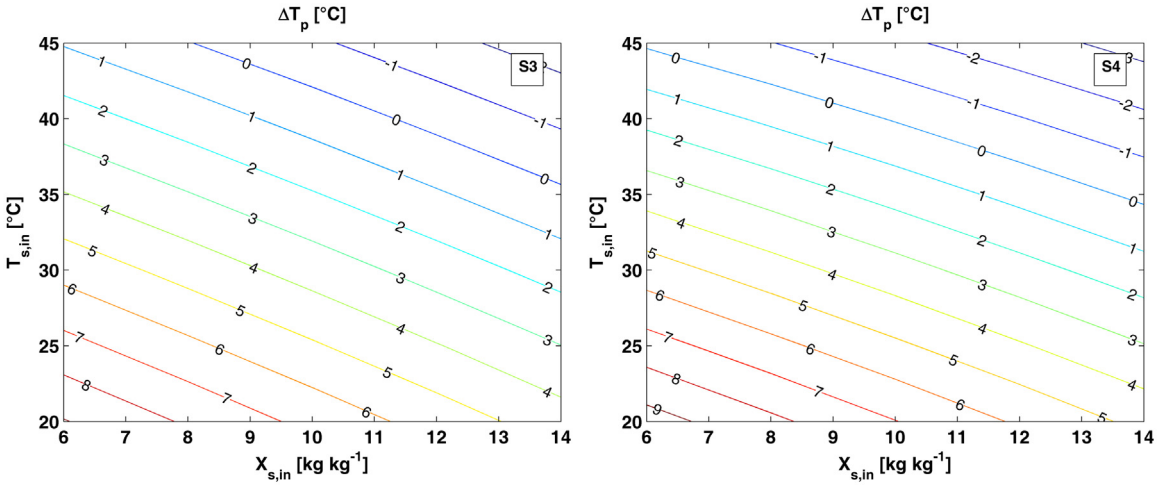

Fig. 11. Numerical results in conditions S3 and S4 (Table 4).

9. Conclusions

In this work an indirect evaporative cooler for data center applications has been investigated. A new indirect evaporative cooling system model has been developed, including effects of secondary air humidification in the inlet plenum and surface wettability factor, as a function of working conditions. It is shown the model can properly predict system performance in a wide range of operating conditions and also outside the calibration range. The indirect evaporative cooling system can provide a significant reduction of primary air temperature. Based on numerical simulations, in case of data center temperature of 35 °C, ΔT_p is around 6 °C in case of hot and humid outdoor conditions ($T_{s,in}$ = 40 °C and $X_{s,in}$ = 14 g kg^{-1}) and it can reach 17 °C in case of cold and dry outside air ($T_{s,in}$ = 20 °C and $X_{s,in}$ = 6 g kg^{-1}).

Acknowledgments

The authors would like to acknowledge Mr Leone and Mr Bawa of Recuperator S.p.A. for the economical and technical support.

References

[1] Khosrow Ebrahimi, Gerard F. Jones, Amy S. Fleischer, A review of data center cooling technology, operating conditions and the corresponding low-grade waste heat recovery opportunities, Renew. Sustain. Energy Rev. 31 (2014) 622–638.
[2] Hainan Zhang, Shuangquan Shao, Hongbo Xu, Huiming Zou, Changqing Tian, Free cooling of data centers: a review, Renew. Sustain. Energy Rev. 35 (2014) 171–182.
[3] Ward Van Heddeghem, Sofie Lambert, Bart Lannoo, Didier Colle, Mario Pickavet, Piet Demeester, Trends in worldwide ICT electricity consumptionfrom 2007 to 2012, Comput. Commun. 50 (September (1)) (2014) 64–76.
[4] ASHRAE Thermal Guidelines for Data Processing Environments – Expanded Data Center Classes and Usage Guidance 2011.
[5] Zhiyin Duan, Changhong Zhan, Xingxing Zhang, Mahmud Mustafa, Xudong Zhao, Behrang Alimohammadisagvand, Ala Hasan, Indirect evaporative cooling: past, present and future potentials, renewable and sustainable energy reviews, Renew. Sustain. Energy Rev. 16 (December (9)) (2012) 6823–6850.
[6] J. Lin, K. Thu, T.D. Bui, R.Z. Wang, K.C. Ng, K.J. Chua, Study on dew point evaporative cooling system with counter-flow configuration, Energy Convers. Manage. 109 (February (1)) (2016) 153–165.
[7] X.C. Guo, T.S. Zhao, A parametric study of an indirect evaporative air cooler, Int. Commun. Heat Mass Transfer 109 (February (2)) (1998) 217–226.
[8] N.J. Stoitchkov, G.I. Dimitrov, Effectiveness of crossflow plate heat exchanger for indirect evaporative cooling: efficacité des échangeurs thermiques à plaques, à courants croises pour refroidissement indirect évaporatif, Int. J. Refrig. 21 (September (6)) (1998) 463–471.
[9] I.L. Maclaine-cross, P.J. Banks, General theory of wet surface heat exchangers and its application to regenerative evaporative cooling, J. Heat Transfer 21 (August (3)) (1981) 579–585.
[10] Sergey Bolotin, Borys Vager, Vladimir Vasilijev, Comparative analysis of the cross-flow indirect evaporative air coolers, Int. J. Heat Mass Transfer 88 (September) (2015) 224–235.
[11] F.J. Rey Martínez, E. Velasco Gómez, R. Herrero Martín, J. Martínez Gutiérrez, F. Varela Diez, Comparative study of two different evaporative systems: an indirect evaporative cooler and a semi-indirect ceramic evaporative cooler, Energy Build. 36 (July (7)) (2004) 696–708.
[12] Chengqin Ren, Hongxing Yang, An analytical model for the heat and mass transfer processes in indirect evaporative cooling with parallel/counter flow configurations, Int. J. Heat Mass Transfer 49 (3–4) (2006) 617–627.
[13] Ghassem Heidarinejad, Shahab Moshari, Novel modeling of an indirect evaporative cooling system with cross-flow configuration, Energy Build. 92 (April (1)) (2015) 351–362.
[14] Ala Hasan, Indirect evaporative cooling of air to a sub-wet bulb temperature, Appl. Therm. Eng. 30 (November (16)) (2010) 2460–2468.
[15] Shyr Tzer Hsu, Zalman Lavan, William M. Worek, Optimization of wet-surface heat exchangers, Energy 14 (November (11)) (1989) 757–770.
[16] Sergey Anisimov, Demis Pandelidis, Andrzej Jedlikowski, Vitaliy Polushkin, Performance investigation of a M (Maisotsenko)-cycle cross-flow heat exchanger used for indirect evaporative cooling, Energy 14 (November (1)) (2014) 593–606.
[17] Demis Pandelidis, Sergey Anisimov, William M. Worek, Paweł Drąg, Comparison of desiccant air conditioning systems with different indirect evaporative air coolers, Energy Convers. Manage. 117 (June (1)) (2016) 375–392.
[18] Shahab Moshari, Ghassem Heidarinejad, Aida Fathipour, Numerical investigation of wet-bulb effectiveness and water consumption in one-and two-stage indirect evaporative coolers, Energy Convers. Manage. 108 (January (15)) (2016) 309–321.
[19] Stefano De Antonellis, Cesare Maria Joppolo, Paolo Liberati, Samanta Milani, Luca Molinaroli, Experimental analysis of a cross flow indirect evaporative cooling system, Energy Build. 121 (June (1)) (2016) 130–138.
[20] DIN EN ISO 5167-2 Standards, Measurement of fluid flow by means of pres-sure differential devices inserted in circular cross-section conduits running full—Part 2: Orifice plates (ISO 5167-2:2003).

[21] Stefano De Antonellis, Manuel Intini, Cesare Maria Joppolo, Desiccant wheels effectiveness parameters: correlations based on experimental data, Energy Build. 103 (September (15)) (2015) 296–306, http://dx.doi.org/10.1016/j.enbuild.2015.06.041, ISSN 0378-7788.
[22] Stefano De Antonellis, Manuel Intini, Cesare Maria Joppolo, Luca Molinaroli, Francesco Romano, Desiccant wheels for air humidification: an experimental and numerical analysis, Energy Convers. Manage. 106 (December) (2015) 355–364, http://dx.doi.org/10.1016/j.enconman.2015.09.034, ISSN 0196-8904.
[23] ISO IEC Guide 98-3, Uncertainty of Measurement—Part 3: Guide to Expression of Uncertainty in Measurement, International Organization for Standardization, ISO IEC Guide 98-3, Geneva Switzerland, 2008.
[24] ASHARE Handbook, HVAC Systems and Equipments, Atlanta, 2012, Chapter 41.
[25] Nian Xiao, Qiang Zhang, Phillip M. Ligrani, Rajiv Mongia, Thermal performance of dimpled surfaces in laminar flows, Int. J. Heat Mass Transfer 52 (March (7–8)) (2009) 2009–2017.
[26] Prashant Kumar, Alok Kumar, Sunil Chamoli, Manoj Kumar, Experimental investigation of heat transfer enhancement and fluid flow characteristics in a protruded surface heat exchanger tube, Exp. Therm. Fluid Sci. 71 (February) (2016) 42–51.